# Isophote Properties as Features for Object Detection

Jeroen Lichtenauer, Emile Hendriks, Marcel Reinders
Delft University of Technology, Information and Communication Theory Group
Mekelweg 4, Delft, The Netherlands
{J.F.Lichtenauer, E.A.Hendriks, M.J.T.Reinders}@ewi.tudelft.nl

## Abstract

*Usually, object detection is performed directly on (normalized) gray values or gray primitives like gradients or Haar-like features. In that case the learning of relationships between gray primitives, that describe the structure of the object, is the complete responsibility of the classifier. We propose to apply more knowledge about the image structure in the preprocessing step, by computing local isophote directions and curvatures, in order to supply the classifier with much more informative image structure features. However, a periodic feature space, like orientation, is unsuited for common classification methods. Therefore, we split orientation into two more suitable components. Experiments show that the isophote features result in better detection performance than intensities, gradients or Haar-like features.*

## 1. Introduction

In order to evaluate the presence of an object in an image, relevant and robust properties of the image must be extracted that can be processed to classify or compare objects. One of the most popular features for object detection has been information about the edges, as used by the well known Chamfer Matching technique [1] and the face recognition method in [2]. Edges contain information about the shape, but they cannot describe smooth surfaces. The shape of these surfaces is visible only because of shading and reflections [3]. Moreover, highly curved surfaces have approximately constant orientation of shading under varying lighting directions [4]. Isophotes follow constant intensity and therefore follow object shape both around edges as well as smooth surfaces. As such they are closed curves within the image.

A totally differentiable curve can be completely described at any point $a$ on the curve by the Taylor expansion $\alpha(s)$ of the curve parameterized by arc length $s$:

$$\alpha(s) = \sum_{n=0}^{\infty} \frac{\alpha^{(n)}(a)}{n!}(s-a)^n \qquad (1)$$

Here, $\alpha(s)$ is a two dimensional vector of the spatial coordinates of the curve at position $s$, $a$ is the point on the curve where all curve derivatives are measured and $\alpha^{(n)}(a)$ is the $n$th derivative of $\alpha$ at point $a$. Isophotes are not necessarily totally differentiable, however, we will only use the first two derivatives and assume that these exist:

$$\begin{aligned}\tilde{\alpha}(s) &= \alpha(a) + \alpha'(a)(s-a) \\ &\quad + \frac{1}{2}\alpha''(a)(s-a)^2 + R \end{aligned} \qquad (2)$$

where $\alpha'(a)$ is the tangent vector at $a$, $\alpha''(a)$ is directly related to curvature $\kappa$ and $R$ contains all higher order terms that are discarded when only direction and curvature are used. We further assume that the tangent and curvature change smoothly over the curve. This implies that isophotes can be described by a sparse set of directions and curvatures. Isophote direction and curvature can be computed directly from gray images [5].

Isophote properties have been used for object detection before. Froba and Kublbeck have used isophote orientation as features for face detection in [6] where they computed an average face model and used angular distances to obtain a similarity measure. Freeman and Roth have used orientation histograms for hand gesture recognition [7], Ravela and Hanson have used histograms of both isophote orientations and curvatures to compare two faces [8] and Maintz et al. [9] have used curvature features to detect ridges in CT/MR images of the human brain. Recently, Froba and Ernst [10] have used the Census Transform [11] as features for face detection. This transform also captures local image structure information. It can distinguish 511 possible local shapes. Apart from detection, isophotes have also been used for image segmentation [12].

Instead of computing isophote (or histogram) similarities to an (average) object model or using an exhaustive

amount of structure features, we propose to use both orientations and curvatures directly as features for training a classifier. To make orientation suitable for classification it is further decomposed into a symmetric and a binary feature. Furthermore, we include a different approach for computing the isophote properties, using gradient structure tensor smoothing. We evaluate the performance of isophote orientation and curvature as object descriptors by applying them to face detection, since face detection is a well studied object detection problem for which a lot of experimental data and results are available.

## 2 Isophote Orientation and Curvature Features

An important parameter for calculating isophote properties is the scale $\sigma_s$ which defines the detail of the structure that is described by the isophotes. Given $\sigma_s$ there are two distinct methods to compute the isophote properties. We shall refer to these methods as the 'direct isophote' (I-) and 'structure tensor' (T-) method respectively.

### 2.1 Direct Isophote Properties

In the direct method, regularized first and second order derivatives are applied directly at scale $\sigma_s$. The local isophote direction $\phi_i$, is given by

$$\phi_i = \arg(D_y - jD_x), \phi_i \in [0, 2\pi) \tag{3}$$

where $D_x$ and $D_y$ are the first order derivatives of the image in horizontal and vertical direction respectively. In the experiments presented in this paper, the derivatives are calculated using Gaussian regularization with $\sigma_s = 1.5$ pixels. $\phi_i$ is directed along the isophote in the direction that keeps the brighter side at the right. On a uniformly colored surface, the brighter side depends on the illumination direction. This can cause a $\pi$ rad ambiguity, making $\phi_i$ bimodal. Also around ridges $\phi_i$ flips $\pi$ rad, causing multimodality when the image is not perfectly registered. Because multimodal classes are more difficult to classify using standard methods, the sign is split from the direction:

$$\theta_i = \phi_i (\text{mod } \pi), \theta_i \in [0, \pi) \tag{4}$$

$$\gamma_i = \begin{cases} 1, & D_x \geq 0 \\ -1, & D_x < 0 \end{cases} \tag{5}$$

$\theta_i$ and $\gamma_i$ are shown in figure 1 (b) and (e), respectively, for concentric circles with Gaussian noise.

Curvature, $\kappa = 1/r$, is defined as the rate of change of direction along a curved line, with $r$ the radius of a circle that has identical curvature. Local isophote curvature $\kappa_i$ can be computed in an image according to [5]

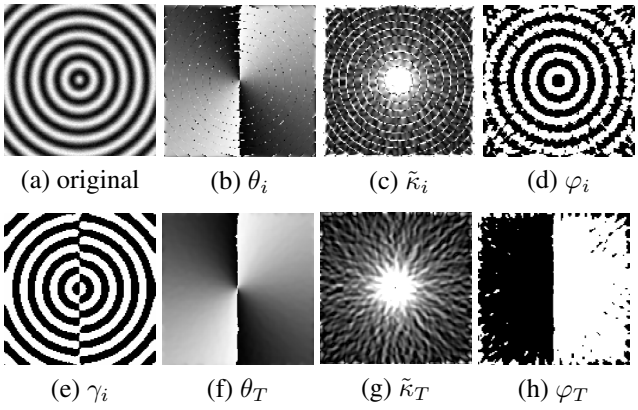

(a) original (b) $\theta_i$ (c) $\tilde{\kappa}_i$ (d) $\varphi_i$

(e) $\gamma_i$ (f) $\theta_T$ (g) $\tilde{\kappa}_T$ (h) $\varphi_T$

Figure 1. Isophote properties for a 128x128pixel image of concentric circles with i.i.d. Gaussian additive noise. (a) original image. (b-e) direct isophote properties. (f-h) GST properties. White corresponds to high, black to low values

$$\kappa_i = \frac{d\theta_i}{ds} = \frac{-(D_y^2 D_{xx} - 2D_x D_y D_{xy} + D_x^2 D_{yy})}{(D_x^2 + D_y^2)^{3/2}} \tag{6}$$

The sign of $\kappa_i$ depends on the intensity at the outer side of the curve. It is positive for a brighter outer side. To prevent multi-modal features, we separate the sign, $\varphi_i$, from the curvature:

$$\tilde{\kappa}_i = |\kappa_i| \tag{7}$$

$$\varphi_i = \begin{cases} 1, & \kappa_i \geq 0 \\ -1, & \kappa_i < 0 \end{cases} \tag{8}$$

$\tilde{\kappa}_i$ and $\varphi_i$ are shown in figure 1 (c) and (d), respectively, for concentric circles with Gaussian noise.

The difficulty with using curvature as a feature is that it can take on any value between $-\infty$ and $\infty$ and curvature difference is not proportional to similarity. Classifiers generally have great difficulty with such features. Therefore, we first transform the feature space of $\tilde{\kappa}_i$ to a space where it is more uniformly distributed, by mapping $\tilde{\kappa}_i$ with its Cumulative Distribution Function (CDF) for i.i.d. Gaussian noise $F_X(\tilde{\kappa}_i)$:

$$\hat{\kappa} = F_X(\tilde{\kappa}) = \int_{-\infty}^{\tilde{\kappa}} f_X(\tilde{\kappa}) dx \tag{9}$$

$f_X(\tilde{\kappa}_i)$ is estimated by computing $\tilde{\kappa}_i$ over an image with 300x300 Gaussian distributed pixels.

### 2.2 Gradient Structure Tensor Properties

As can be seen in figure 1 (b, c), the isophote orientation and curvature suffer from singularities. This is because they

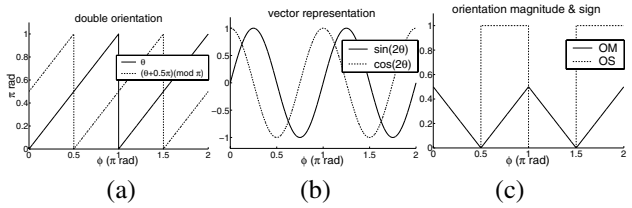


Figure 2. Three alternative orientation representations. In (a) double orientation. (b) vector representation, $\sin(2\theta)$ and $\cos(2\theta)$. (c) orientation magnitude (OM) and orientation sign (OS)

are not defined for pixels with zero gradient. A solution is to use the orientation tensor representation, as explained in [5]. In this approach, $D_x$ and $D_y$ are first computed at a small scale, from which the gradient tensor $\mathbf{G}$ is computed. The tensor components are smoothed over a neighborhood, obtaining the average tensor $\overline{\mathbf{G}}$, called the Gradient Structure Tensor (GST):

$$\overline{\mathbf{G}} = \begin{bmatrix} \overline{\mathbf{G}_{11}} & \overline{\mathbf{G}_{12}} \\ \overline{\mathbf{G}_{21}} & \overline{\mathbf{G}_{22}} \end{bmatrix} = \begin{bmatrix} \overline{D_x^2} & \overline{D_x D_y} \\ \overline{D_x D_y} & \overline{D_y^2} \end{bmatrix}$$

where the bar ($\overline{\bullet}$) denotes the result after applying a smoothing operator with scale $\sigma_s$. In the experiments, the small-scale horizontal and vertical derivatives are computed by convolution with $[\frac{1}{2}\ 0\ -\frac{1}{2}]$ and $[-\frac{1}{2}\ 0\ \frac{1}{2}]^T$, respectively. Tensor smoothing is performed with a Gaussian filter with $\sigma_s = 1.5$. The smooth GST can be used to compute isophote properties with much less singularities. GST orientation $\theta_T$ is calculated by

$$\theta_T = \frac{1}{2}\arctan\left(\frac{2\overline{\mathbf{G}}_{12}}{\overline{\mathbf{G}}_{11} - \overline{\mathbf{G}}_{22}}\right) + \frac{1}{2}\pi, \theta_T \in (0, \pi] \quad (10)$$

The result is shown in figure 1 (f). GST curvature $\kappa_T$ is calculated by [5]

$$\kappa_T = -\cos(\theta_T)\frac{\partial \theta_T}{\partial x} - \sin(\theta_T)\frac{\partial \theta_T}{\partial y} \quad (11)$$

with

$$\frac{d\theta_T}{dx} = \Re\left\{\frac{1}{2} j e^{(-j2\theta_T)}\left(\frac{\partial cos(2\theta_T)}{\partial x} + j\frac{\partial sin(2\theta_T)}{\partial x}\right)\right\}$$
$$\frac{d\theta_T}{dy} = \Re\left\{\frac{1}{2} j e^{(-j2\theta_T)}\left(\frac{\partial cos(2\theta_T)}{\partial y} + j\frac{\partial sin(2\theta_T)}{\partial y}\right)\right\}$$

where $\Re(c)$ is the real part of $c$. $\partial sin(\theta_T)$ and $\partial cos(\theta_T)$ to $x$ and $y$ are calculated by convolution with $[\frac{1}{2}\ 0\ -\frac{1}{2}]$ and $[-\frac{1}{2}\ 0\ \frac{1}{2}]^T$, respectively. $\tilde{\kappa}_T = |\kappa_T|$ and $\varphi_T$, see figure 1 (g, h), are also separated to prevent multi-modal features. The positive sign of $\kappa_T$ now corresponds to curves that have their outer side directed towards the right side of the image, as can be seen from the signs in fig. 1 (h). Also $\tilde{\kappa}_T$ is transformed by its CDF in Gaussian noise using equation 9 to obtain $\hat{\kappa_T}$ as a feature.

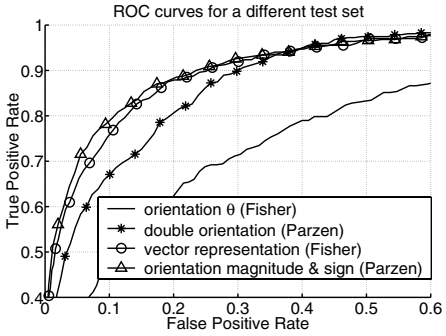


Figure 3. Comparison of orientation representations. Resulting ROC curves for the testset that is explained in section 3

### 2.3 Orientation Features

The orientation $\theta$ is discontinuous with a jump at every $\pi$ rad. This property is not well suited for classification because it will split classes where they cross $\theta = \pi$. To reduce this problem the orientation can be represented by two features. Three different representations are shown in figure 2: double orientation (a) where the discontinuities are at different positions, vector representation (b) and orientation magnitude and sign (OM and OS) (c) computed by

$$OM = |\theta/\pi - 0.5| \quad (12)$$
$$OS = \begin{cases} 0, & \theta < \frac{1}{2}\pi \\ 1, & \theta \geq \frac{1}{2}\pi \end{cases} \quad (13)$$

where OM is symmetric and OS indicates the side of the symmetric OM. Note that OM corresponds to 'horizontalness'.

To select the best representation, an experiment is performed similar to the experiments explained in section 3. A feature set was obtained by concatenating the features resulting from the direct isophote and GST orientations. The best ROC curves of three different classifiers are shown in figure 3. The vector and magnitude/sign representations provide the best results. Furthermore, the fact that OM features are different from OS features can give this representation an advantage when it is used in combination with other features, since maybe only either OM or OS is interesting to combine with certain other features, while the two components of the vector representation do not have any distinct property to offer over the other one. Therefore, we have used the OM/OS orientation representation in the experiments of section 3.

## 3 Experimental Results

We will compare isophote features to pixel, gradient and Haar-like features, all computed after histogram equal-

Table 1. Feature set names and descriptions

| feature set name | set size | description |
|---|---|---|
| **Illumination:** see fig. 4 | | |
| NL361 | 19x19=361 | All Normalized (histogram equalization) Luminance values |
| NL81 | 9x9=81 | Grid of pixels selected after Gaussian smoothing with standard deviation (std.) of 1 pixel and histogram equalization |
| **Gradient:** | | |
| GH | 9x9=81 | Horizontal gradient magnitudes from the histogram equalized face using filtering with Gaussian derivatives, std. 1.5 pixels |
| GV | 9x9=81 | Same as GH but vertical |
| G | 9x9=81 | $G = \sqrt{GH^2 + GV^2}$, used instead of GH and GV in the experiments with all feature sets |
| **Haar-like features:** | | |
| H2H | 9x9=81 | Horizontal differences |
| H2V | 9x9=81 | Vertical differences |
| H3H | 9x9=81 | Horizontal peak filter |
| H3V | 9x9=81 | Vertical peak filter |
| H4 | 9x9=81 | Diagonal filter |
| **Isophote features:** see fig. 4 | | |
| IDS | 9x9=81 | Isophote Direction Sign ($\gamma_i$) |
| IOM | 9x9=81 | Isophote Orientation Magnitude derived from $\theta_i$ |
| IOS | 9x9=81 | Isophote Orientation Sign derived from $\theta_i$ |
| TOM | 9x9=81 | GST Orientation Magnitude derived from $\theta_T$ |
| TOS | 9x9=81 | GST Orientation Sign derived from $\theta_T$ |
| IC | 9x9=81 | Normalized Isophote Curvature $\hat{\kappa}_i$ |
| ICS | 9x9=81 | Isophote Curvature Sign ($\varphi_i$) |
| TC | 9x9=81 | Normalized GST Curvature ($\hat{\kappa}_T$) |
| TCS | 9x9=81 | GST Curvature Sign ($\varphi_T$) |

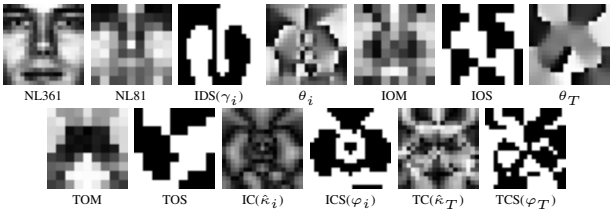


Figure 4. Features and orientations of a face image.

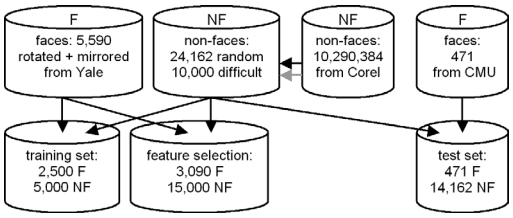


Figure 5. Datasets used in the experiments. By randomly drawing from two face (F) sets and one non-face (NF) set, three non-overlapping datasets are obtained. The gray arrow denotes selection based on high face detector output

ization, while the isophote features are computed without histogram equalization since they are invariant to contrast.

### 3.1 Features

The features sets that will be compared are shown in table 1. The Haar-like features, as used in [13], are computed at approximately the same scale as the other features. The filter sizes for the horizontal and vertical filters are 2 by 4 pixels. The size of the diagonal filter is 4 by 4. Because these filters are even-sized and the face patches are odd-sized, the center results are averaged to obtain a symmetrical odd-sized feature set. With each of the five filters a feature set of 9x9 values is obtained from a normalized 19x19 image patch. Note that Haar-like features usually also include longer versions of the filters. These are omitted here, as they are equivalent to combinations of the short filters.

### 3.2 Datasets

The databases used in the experiments are shown in figure 5. The face examples that are used for training and feature selection are taken from the Yale Face Database B [14]. This database consists of images of 10 different subjects taken under a discrete set of different angles and illuminations. To obtain more robustness to rotations, the images were randomly rotated by a uniform distribution between -20 and 20 degrees. The rotated images were re-scaled and face patches of 19 by 19 pixels were cut out and finally mirrored to obtain more samples. Faces that were close to the border of the image were left out. One part of these samples was used for training and the other for feature set selection. For testing we used the CMU Test Set 1 [15], which consists of images of scenes containing one or more (near) frontal human faces. The faces were re-scaled and cut out to obtain a total of 471 face patches. As non-face examples image patches were obtained at different scales from images of the Corel image database that did not contain any faces. 10,000 of the selected patches were the ones that looked most similar to a face according to a face classifier using quadratic Bayes classification on a combination of isophote features and luminance values.

### 3.3 Classifiers

All features are normalized to have standard deviation 1 over the entire training set. Three different classifiers were used: the linear Fisher discriminant, quadratic Bayes (Normal-based) and unbounded Bayes (Parzen density). See [16] for more details on these classification methods. With the quadratic classifier Principle Component Analysis (PCA) is performed on the face class features (similar to [17]) to select the most important eigenvectors that, together, contribute to 99% of the total variance. The Parzen density classifier is not practical since the classification is very slow but it has good performance on complex, non-linear class distributions. Note that these are single-stage classifiers, while in practical situations a cascade of classifiers combined with boosting, like described in [13], is applied to obtain real-time speed. Since we want to evaluate the features themselves, speed is not regarded in these experiments.

To select an optimal feature set, a feature-set selection procedure is followed. By forward selection, at each step

Table 2. Feature selection and classification results. The selected feature sets are in the order in which they were selected. For the Normal-based classifier the second number of features is the number of principle components. The area's above the ROC curves are computed both for the feature selection dataset and the test set

| feature type | selected sets, if applicable otherwise all used sets | nr. of feat. | selection ROC | test ROC |
|---|---|---|---|---|
| **Normal-based:** | | | | |
| NL361 | NL361 | [361,213] | 0.0133 | 0.160 |
| NL81 | NL81 | [81,69] | 0.0258 | 0.115 |
| Gradient | GH, GV | [162,49] | 0.0210 | 0.209 |
| Haar-like | H2V, H3V | [162,111] | 0.0317 | 0.263 |
| Isophote | TOM, ICS, TOS, IOS, IDS | [405,358] | $5.81\times10^{-4}$ | 0.0323 |
| all features | G, ICS, TOM, IC, H2H, TOS | [486,347] | $2.01\times10^{-4}$ | 0.0827 |
| **Fisher:** | | | | |
| NL361 | NL361 | [81] | 0.0578 | 0.112 |
| NL81 | NL81 | [81] | 0.0989 | 0.112 |
| gradient | GH, GV | [162] | 0.0613 | 0.0864 |
| Haar-like | H2V, H3H, H3V, H2H, H4 | [405] | 0.0594 | 0.0905 |
| isophote | TOM, ICS, IOM, IC, TOS, TC, IDS, IOS, TCS | [729] | $3.62\times10^{-3}$ | 0.0627 |
| all features | TOM, G, ICS, IC, H2V, IOM, NL81, TOS, IOS, TC, H3H, TCS, H2H | [972] | $1.09\times10^{-3}$ | 0.0446 |
| **Parzen:** | | | | |
| NL361 | NL361 | [361] | 0.0066 | 0.172 |
| NL81 | NL81 | [81] | 0.0122 | 0.249 |
| gradient | GH, GV | [162] | 0.1023 | 0.242 |
| Haar-like | H2H, H2V, H3V | [192] | $1.33\times10^{-3}$ | 0.188 |
| isophote | TOM, ICS, IOS, TCS | [324] | $1.98\times10^{-4}$ | 0.0542 |
| all features | G, ICS, TOM, TOS | [324] | $7.96\times10^{-5}$ | 0.0585 |

the feature set is added to the existing set that minimizes the area above the ROC curve until there is no feature set left that results in a decrease of the ROC area. The PCA procedure before the Normal-based classifier training was applied after combining the selected feature sets.

The results in table 2 show the performance on the feature selection data set and the test set. The feature types of the experiments correspond to the type of feature sets that the feature selection procedure was limited to. See table 1 for more details on the feature sets. In this way, the luminance, gradient, Haar-like and isophote feature sets are tested individually. The selected feature sets are shown in the order of selection. The 'all features' experiments exclude NL361, and GH and GV are replaced by G (see table 1). The resulting ROC curves of the combined sets are shown in figure 6. These results are for the classifier that resulted in the smallest area above the curve.

### 3.4 Discussion

The isophote properties result in better classification (smaller area above ROC curve) than the normalized luminance values, gradients or Haar-like features, for all three classifiers. The combination of all features resulted in a slightly better classification over the selection set, but on the test set the best result was obtained with the isophote properties alone, indicating that isophote properties generalize better. For the classifiers using all features, most of the selected sets were isophote properties. This indicates that the isophote properties capture the most important information about the structure of the face and luminance and gradient magnitudes are less essential.

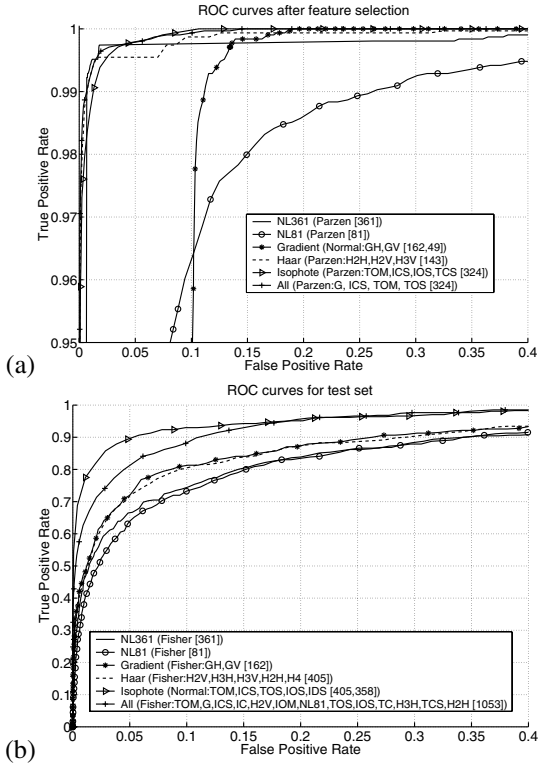


Figure 6. ROC curves. (a) at the end of feature set selection, (b) classification on the different test set. The results are for the classifier that resulted in the smallest area above the curve.

There is no clear preference between GST and direct isophote features, though. With all three classifiers, pairs of similar features for the two different approaches are combined to improve performance, suggesting that the two approaches capture different structural information. From the Haar-like features, only two or three sets were selected for Normal-based and Parzen classification, while much more sets were selected from the isophote properties. Apparently, the Haar-like features have more redundancy than the isophote features. The Parzen classifier nearly always outperforms the other two classifiers on the feature selection set but not on the test set. This is because Parzen density is more complex, hence more sensitive to 'over-training' and, therefore, does not generalize well.

## 4 Conclusions and Future work

We proposed to use a combination of isophote properties to obtain a compact and descriptive representation of image structure that is invariant to contrast and robust to illumination changes. Furthermore, to make orientation features suitable for classification they are separated into a symmetrical and a binary feature. We applied it to face detection

and compared the isophote features to Haar-like features, gradients and normalized luminance values, which are often used for face detection. The experiments show a better classification performance, especially when applied to a separate test set, which indicates better generalization. The direct and the GST approach for obtaining isophote features supplement each other, indicating that they capture different information about the object structure. Only single-scale-features were used here, while all features can also be computed at other scales to obtain even better classification performance. In these experiments, speed is not taken into account. The Haar-like features can be computed efficiently using the integral image, as explained in [13], while the isophote features in this paper are computed using Gaussian filtering, trigonometric and modulo calculations, which slow down the computation significantly. One possibility is to compute the isophote properties from an image pyramid with only a few scales and then apply nearest neighbour interpolation on the closest scale(s) to obtain the features on scales in between. The best application for isophote features seems to be object tracking, where the approximate scale of the object can be predicted from the previous observations. A multi-scale search needs to be performed only at initialization and features need to be re-computed only where the local image content has changed.

## References


[1] H.G. Barrow, J.M. Tenenbaum, R.C. Bolles, and H.C. Wolf, "Parametric correspondence and chamfer matching: Two new techniques for image matching," in *IJCAI77*, 1977, pp. 659–663.

[2] Yongsheng Gao and Maylor K.H. Leung, "Face recognition using line edge map," *PAMI*, vol. 24, no. 6, pp. 764–779, 2002.

[3] J.J. Koenderink and A.J. van Doorn, *Shape From Shading*, chapter Photometric Invariants Related to Solid Shape, MIT Press, Cambridge, MA, USA, 1989.

[4] H.F. Chen, P.N. Belhumeur, and D.W. Jacobs, "In search of illumination invariants," in *CVPR00*, 2000, pp. I: 254–261.

[5] M. van Ginkel, J. van de Weijer, P.W. Verbeek, and L.J. van Vliet, "Curvature estimation from orientation fields," in *ASCI'99*, June 1999, pp. 299–306.

[6] B. Froba and C. Kublbeck, "Robust face detection at video frame rate based on edge orientation features," in *AFGR02*, 2002, pp. 327–332.

[7] W. Freeman and M. Roth, "Orientation histogram for hand gesture recognition," in *Int'l Workshop on Automatic Face- and Gesture-Recognition*, 1995, pp. 296–301.

[8] S. Ravela and Allen Hanson, "On multi-scale differential features for face recognition," in *Vision Interface*, Ottawa, June 2001.

[9] J.B.A. Maintz, P.A. van den Elsen, and M.A. Viergever, "Evaluation of ridge seeking operators for multimodality medical image matching," *PAMI*, vol. 18, no. 4, pp. 353–365, April 1996.

[10] B. Froba and A. Ernst, "Face detection with the modified census transform," in *Sixth IEEE International Conference on Automatic Face and Gesture Recognition*, May 2004, pp. 91–96.

[11] R. Zabih and J. Woodfill, "Non-parametric local transforms for computing visual correspondence," in *ECCV*, May 1994, vol. B, pp. 151–158.

[12] C. Kervrann, M. Hoebeke, and A. Trubuil, "Isophotes selection and reaction-diffusion model for object boundaries estimation," *IJCV*, vol. 50, no. 1, pp. 63–94, October 2002.

[13] P. Viola and M. Jones, "Rapid object detection using a boosted cascade of simple features," in *CVPR01*, December 2001, vol. 1, pp. 511–518.

[14] A.S. Georghiades, P.N. Belhumeur, and D.J. Kriegman, "From few to many: Illumination cone models for face recognition under variable lighting and pose," *PAMI*, vol. 23, no. 6, pp. 643–660, 2001.

[15] H. A. Rowley, S. Baluja, and T. Kanade, "Neural network-based face detection," *PAMI*, vol. 20, no. 1, pp. 23–38, 1998.

[16] R.O. Duda, P.E. Hart, and D.G. Stork, *Pattern Classification*, Wiley, 2001.

[17] M. Turk and A.P. Pentland, "Face recognition using eigenfaces," in *CVPR91*, 1991, pp. 586–591.